Ionics (2019) 25:4651–4658
https://doi.org/10.1007/s11581-019-03029-x

ORIGINAL PAPER

Synthesis of Co/SnO_2 core-shell nanowire arrays and their electrochemical performance as anodes of lithium-ion batteries

Yu Lei[1] · Ning Du[1] · Wei Liu[1] · Hao Wu[1] · Deren Yang[1]

Received: 22 February 2019 / Revised: 23 April 2019 / Accepted: 24 April 2019 / Published online: 4 July 2019

Abstract

The Co/SnO_2 core-shell nanowire arrays were synthesized via a simple hydrothermal approach and subsequently the deposition of amorphous SnO_2 layer. When used as anode materials of lithium-ion batteries, the Co/SnO_2 core-shell nanowire arrays maintain at 667.9 mAh g^{-1} with the capacity retention of 85.7% after 100 cycles at the current density of 200 mA g^{-1}. For comparison, the discharge capacity of the planar SnO_2 electrodes shows the capacity of 196.3 mAh g^{-1} with the capacity retention of 22.6% after 100 cycles under the same condition. The enhanced electrochemical performance is attributed to the core-shell array nanostructures that can improve the conductivity and buffer the volume changes of tin-based anode during the charge/discharge process.

Keywords SnO_2 · Core-shell nanowire array · Lithium-ion battery · Anode material

Introduction

Recently, the increasing development of portable electronic equipment and electric vehicles puts forward high requirements for the performance of lithium-ion batteries. As the widely used anode material for commercial lithium-ion batteries, graphite has a relatively low theoretical capacity (~ 372 mAh g^{-1}) [1, 2], which greatly limits the application of lithium-ion batteries in high power density devices. So, a novel anode material which possesses higher specific capacity, better safety performance, longer life, and lower cost is in need. Tin-based materials have been regarded as one of the most promising alternative anodes for lithium-ion batteries [3–5]. Among them, the low-cost material, SnO_2, with the high theoretical reversible capacity (~ 782 mAh g^{-1}) and low electrochemical potential of lithium insertion [6, 7], has been regarded as a promising anode material for the next generation lithium-ion batteries. However, similar to other lithium alloy materials, it suffers ~ 300% volume change during the lithium alloy/dealloy process [8], which makes it impossible to be popularized on a large-scale production [9]. To circumvent these issues, designing a new structure might be an effective approach. According to previous reports, a wide variety of SnO_2 nanostructures, such as nanorods [10, 11], nanoflowers [12], nanoflakes [13], porous and hollow structures [14–18], nanotubes [19–21] and core-shell structures [22, 23], were synthesized to address the challenge of volume change during cycling processes. Compared with the conventional structure, the array nanostructured electrodes have better volumetric expansion capacity, charge transfer capacity and structural stability [23–29]. The nano-array structures have several advantages: (1) Nano-sized array anodes can gain better contact between current collector substrate and electrolyte, due to the three-dimensional structure which can offer more spaces for the electrolyte. (2) It can shorten the distance of the diffusion for the ions and electrons, which facilitates the conduction, (3) No binders or conductive additives are needed because of the in situ growth of electrode materials directly onto the current collector substrate. Therefore, the common problems that arise from sluggish charge transfer at the interfaces between the active materials and the binders/additives could be avoided, and this eases the preparation of the electrode structures as well. (4) The better support of array structure contribute to the relaxation of the mechanical stress of electrode materials during the repetitive charge/discharge process [30–33].

✉ Ning Du
86-571-87953190dna1122@zju.edu.cn

[1] State Key Laboratory of Silicon Materials and School of Materials Science and Engineering, Zhejiang University, Hangzhou 310027, People's Republic of China

In this report, we demonstrate Co/SnO_2 core-shell nanowire arrays with Co nanowires as the current collector and SnO_2 as the active material. The good electrical conductivity of Co nanowire matrix can significantly improve the charge transfer capacity of the electrode [34, 35]. Moreover, SnO_2 deposited on the Co nanowires has a high specific surface area, which not only increases the contact area of electrode/electrolyte, but also reserves good strain accommodation for anode materials during charge-discharge cycles. Therefore, the three-dimensional core-shell Co/SnO_2 nanowire arrays are believed to show good electrochemical performance as anode materials of lithium-ion batteries.

Experimental

Synthesis of Co nanowire arrays on Ti substrates

The Co nanowire arrays were grown on Ti substrates by the hydrothermal method described by a previous paper with slight modification [36]. The steps were as follows: 5 mmol $Co(NO_3)_3 \cdot 6H_2O$ and 25 mmol urea were dissolved in a 50-mL deionized water followed by stirring until completely dissolved, and the homogeneous solution and Ti sheets were then transferred into a 100-mL customized hydrothermal reactor, reacting at 95 °C for 3.5 h. After the reaction, the product was rinsed with deionized water and ethanol for several times. Afterwards, it was placed in the tube furnace and kept at 400 °C for 2 h in an argon atmosphere. Finally, the sample was heated at 350 °C for 3 h in hydrogen and/or argon atmosphere and then cooled down to room temperature, and Co nanowire arrays grown on Ti substrates were obtained.

Synthesis of Co/SnO_2 core-shell nanowire arrays

Core-shell Co/SnO_2 nanowire arrays were deposited onto the substrate by RF sputtering with a 99.9% SnO_2 target. The working pressure was 1.0 Pa, and the power was 72 W.

Material characterizations and electrochemical measurement

The morphology and structure of the product were characterized by using X-ray diffraction (XRD, X'PERT, PRO), field emission scanning electron microscope (SEM, S4800, Hitachi), and transmission electron microscope (TEM, Tecnai, G2F30).

CR2025 coin cells, with a metal lithium as the counter electrode and 1 M solution of $LiPF_6$ in ethylene carbonate (EC) and dimethyl carbonate (DMC) (1:1 by volume) as an electrolyte, determined the electrochemical properties of the products. Nickel foam was the supported material, while Celgard 2300 porous composite membrane was a diaphragm of the cell. The assembling of CR2025 coin cells was in a glove box in a high purity argon atmosphere with the lower than 0.1 ppm content of oxygen and water.

Galvanostatic cycling test of the assembled cells was carried out on a Land CT2001A system (Wuhan Blue Electric Technology Co. Ltd) in the potential range of 0.01~3.0 V at a current density of 200 mA/g with the temperature of 25 ± 1 °C.

Results and discussion

Figure 1 shows the XRD spectra of the products along with the preparation. Except for the peaks of Ti on the substrate, the other diffraction peaks are corresponding to the Co $(CO_3)_{0.5}(OH)\ 0.11H_2O$ of the orthogonal crystal system (JCPDS: 48-0083N) (Fig. 1a), CoO (JCPDS: 48-1719m) of the FCC system (Fig. 1b), and Co (JCPDS: 89-4308) of the HCP hexagonal system [37], respectively. The transformation of the XRD spectrum demonstrated that the $Co(CO_3)_{0.5}(OH)0.11H_2O$ was transformed into CoO, and then Co along with the thermal treatment. In addition, there were no obvious diffraction peaks of SnO_2 because of the amorphous structure of SnO_2 after RF sputtering [38].

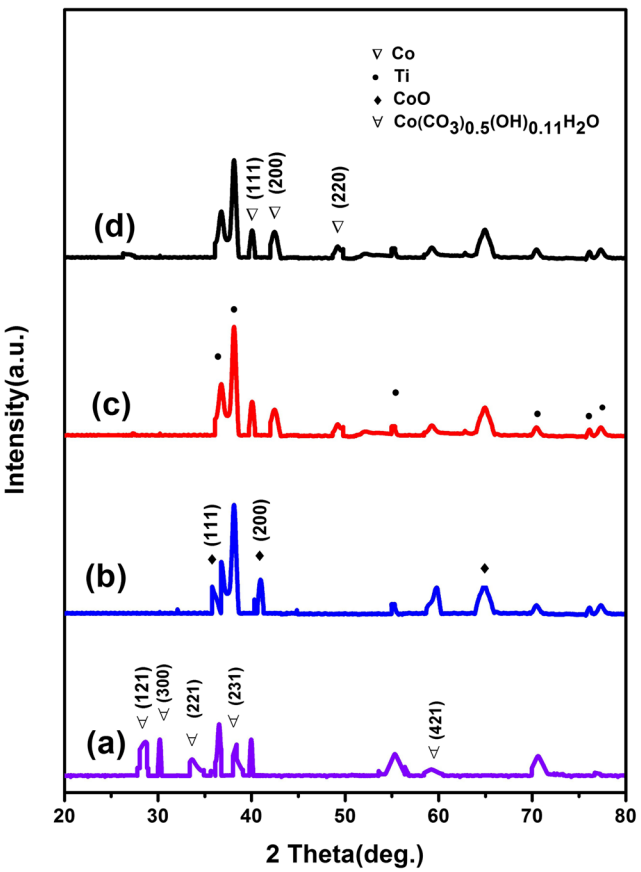

Fig. 1 XRD patterns of Co $(CO_3)_{0.5}(OH)0.11H_2O$ (**a**), CoO (**b**), Co (**c**), and Co/SnO_2 core-shell nanowire array (**d**)

Figure 2a shows the SEM image of products after the hydrothermal reaction. The surface of the nanowires is smooth and essentially grows vertically on the Ti substrate. The heat-treated CoO nanowire arrays are shown in Fig. 2b, with an average diameter of 110 nm, which is smaller than that of its precursor due to the loss of H_2O and CO_2. As shown in Fig. 2c, the average diameter of Co nanowires, which were reduced from CoO nanowires, is further shrunk to 70~80 nm and the surface of the nanowires turns into rough. As SnO_2 was deposited on the surface of Co nanowires, the tip of nanowires gradually becomes "coarse." As shown in Fig. 2d, the average diameter of Co/SnO_2 core-shell nanowire arrays is about 150 nm after the sputtering process.

TEM was employed to further verify the core-shell structure (Fig. 3). It can be seen that a SnO_2 layer with the thickness of ~ 100 nm has been deposited onto the Co nanowires. Figure 3b is a high-resolution TEM (HRTEM) image of an individual Co/SnO_2 nanowire, indicating that the core is crystalline while the shell is amorphous. The lattice fringes with the lattice spacing of 2.4 Å correspond to the {111} planes of Co [39]. Figure 3 c and d are the area-scanning EDX spectra of an individual Co/SnO_2 core-shell nanowire. As shown in Fig. 3d, the Co element, a wedge shape with a thick tail and a sharp tip, is consistent with the morphology of the Co nanowires shown in the SEM image (Fig. 2d). It can be seen that Sn and O are evenly distributed in the shell of the nanowire, indicating that the SnO_2 in the outer layer is uniformly deposited on the surface of Co. The result of TEM analysis further confirms the formation of uniform Co/SnO_2 core-shell structure.

Figure 4 is the SEM images of three-dimensional electrodes with a sputtering time of 5, 10, 15, and 20 min in the DC sputtering power of 72 W. It can be seen that the Co/SnO_2 core-shell nanowires become thicker along with the increasing sputtering time. When the sputtering time is 5 min, the average diameter is about 80 nm; while when the time extends to 10 min, the average diameter increases to 100 nm. As the sputtering time prolonged to 15 min and 20 min, the average diameter of the Co/SnO_2 nanowires is respectively increased to 120 nm and 150 nm. Furthermore, the Co/SnO_2 nanowires transformed into a pillar with a large top and gradually become more and more slender thinning from the head to the tail.

Figure 5 shows the discharge capacity vs. the cycle number for the four electrodes with a sputtering time ranging from 5 to 20 min at the current density of 200 mA/g. When the sputtering time is 5 min, the Co/SnO_2 core-shell nanowires show an initial reversible capacity of 550 mAh g^{-1} and decrease slowly to 500 mAh g^{-1} after 50 cycles. When the sputtering time increases to 10 and 15 min, the initial reversible capacity increases to 650 and 800 mAh g^{-1} due to the increase of the active mass, which decreases slowly to 600 and 750 mAh g^{-1}, respectively. The cycling performance is similar to the above three samples. When the sputtering time increases to 20 min, the Co/SnO_2 core-shell nanowires show the initial capacity of ~ 800 mAh g^{-1} but decrease quickly to 550 mAh g^{-1} after 50 cycles. The excessive SnO_2 would cover the top of the Co nanoarrays, suggesting that there is insufficient space for buffering the volume expansion of the electrode during cycling, leading to the poor cycling performance.

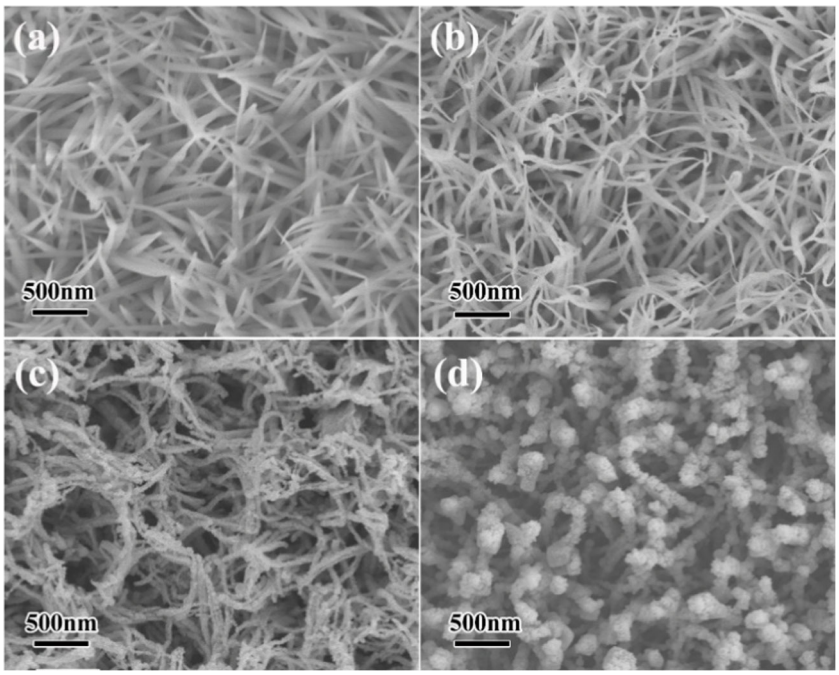

Fig. 2 SEM images of $Co(CO_3)_{0.5}(OH)\ 0.11H_2O$ (**a**), CoO (**b**), Co (**c**), Co/SnO_2 nanowire arrays (**d**)

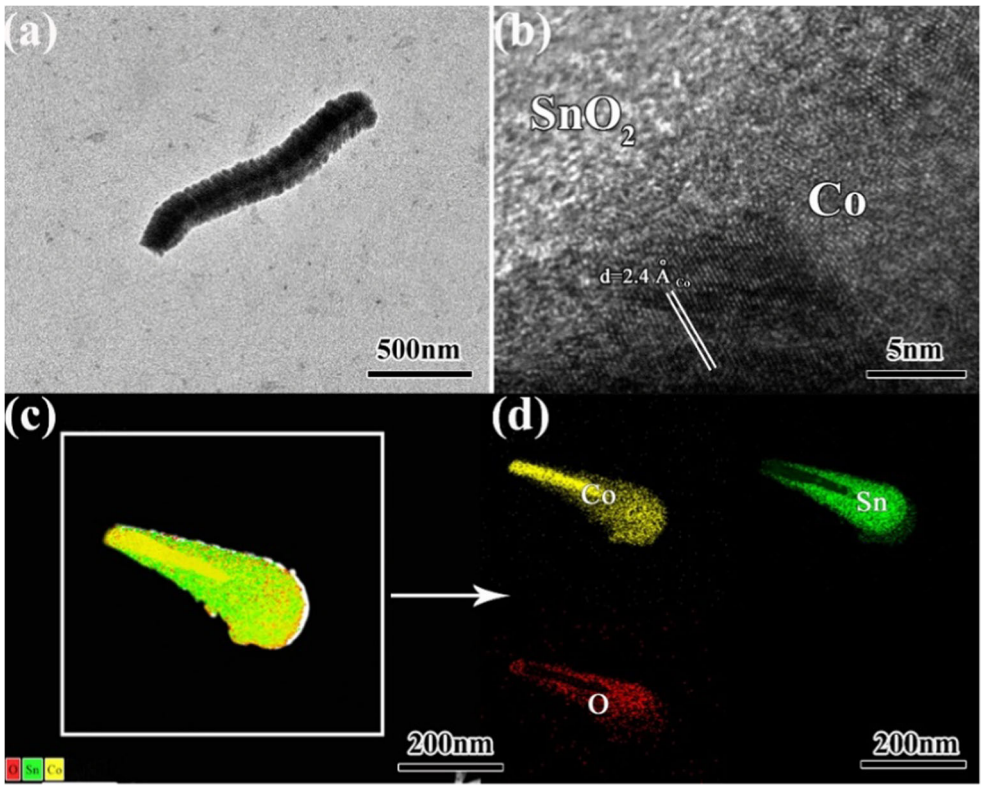

Fig. 3 Morphological and structural characterizations of Co/SnO_2 core-shell nanowire arrays. **a** TEM. **b** HRTEM. **c**, **d** Area-scanning EDX spectra of the Co/SnO_2 core-shell nanowires. As can be seen in **d**, Co is yellow color, Sn is green color, and O is red color

Figure 6a shows the cyclic voltammograms of Co/SnO_2 core-shell nanowire arrays between 0.01 and 3.0 V at a scan rate of 0.1 mV s^{-1}. It can be seen that the curve of the oxidation-reduction potential of SnO_2 is consistent with the previous paper [40]. There is a reduction peak at ~0.8 V, which is related to the decomposition of lithium oxide and the formation of solid electrolyte interface (SEI) layer [41], while the broader peak between 0.1~0.5 V corresponds to the alloying reaction process of Li and Sn, as shown in the reaction Formula (1):

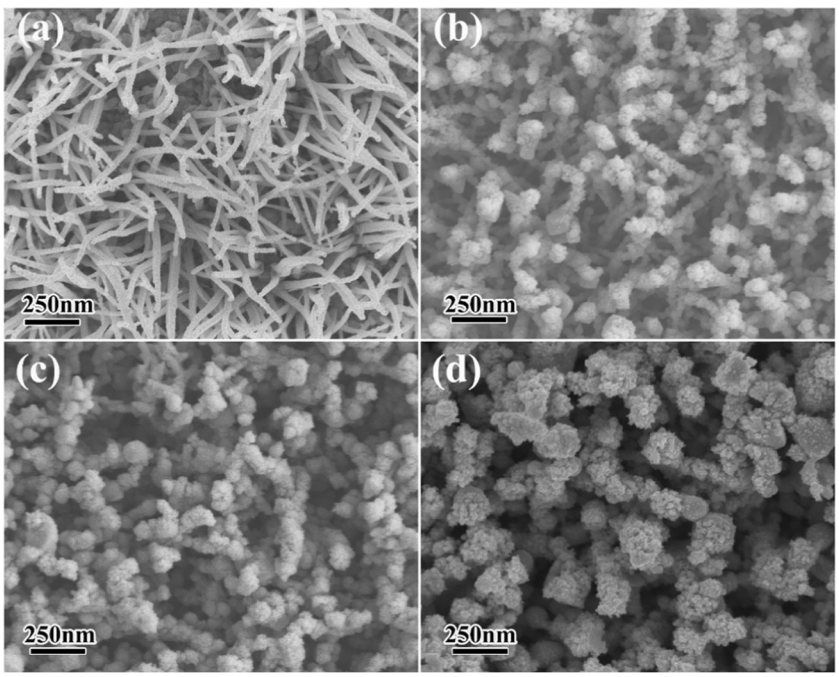

Fig. 4 SEM images of three-dimensional electrodes with a sputtering SnO_2 time of 5 min (**a**), 10 min (**b**), 15 min (**c**), and 20 min (**d**) at the current density of 200 mA/g

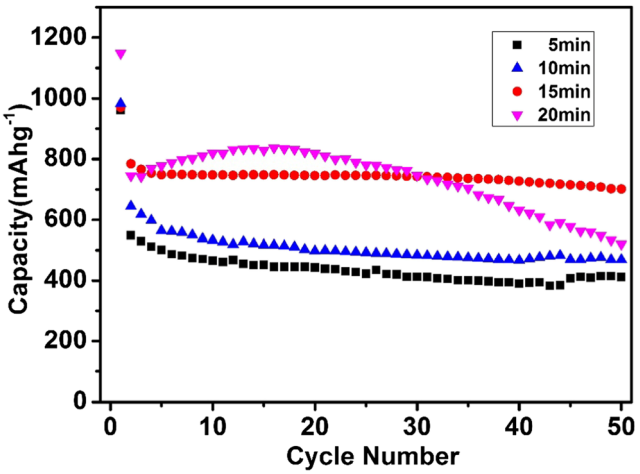

Fig. 5 Discharge capacities versus cycle number of three-dimensional electrodes with a sputtering SnO_2 time of 5 min, 10 min, 15 min, and 20 min

$$xLi^{+} + \mathrm{Sn} + xe^{-} \leftrightarrow Li_xSn \quad (1)$$

The oxidation peak of 0.6 V in the oxidation process refers to the dealloying process of $Li_{4.4}Sn$ [42]. Two peaks of 0.7 and 1.3 V disappear in the second and third cycles, and a small reduction peak arises at ~ 1.2 V. That is because the lithium intercalation of SnO_2 is irreversible, just like the reaction Formula (2):

$$2Li^{+} + 2e^{-} + SnO_2 \rightarrow Li_2O + Sn \quad (2)$$

Therefore, the peaks of SnO_2 do not exist after the first cycle, which are replaced by the oxidation/reduction peaks of Sn. The transformation of SnO_2 to Sn and the irreversibility of Li_2O are the main reason for the low coulombic efficiency in the first cycle [42]. After the first cycle, the curves of each cycle are smooth and almost coincide, which indicate the good reversibility lithiation/delithiation in the subsequent cycles.

Figure 6b shows galvanostatic charge/discharge curves of the as-synthesized materials with the sputtering time of 15 min for the 1st, 2nd, and 100th cycles with the potential window between 0.01~3.0 V, at the current density of 200 mA g^{-1}. There is a "platform" near 0.9 V, which corresponds to the formation of SEI and the irreversible reaction of Li with the SnO_2. This is consistent with the characteristics of the CV curve shown in Fig. 6a. Meanwhile, the different discharge capacity of the first two cycles is related to the irreversible Li_2O. After 100 cycles, the discharge capacity is still ~ 700 mAh g^{-1}, indicating the good cycling stability.

Figure 7a is the charge/discharge capacity curve of the Co/SnO_2 core-shell nanowire arrays versus cycle number at a current density of 200 mA g^{-1}. The reversible capacity maintains at 674.3 mAh g^{-1} after 100 cycles, with the capacity retention of 85.7%. Except for the first cycle, the coulombic efficiency is higher than 94%, indicating that the electrode has good reversibility and good structural stability. Figure 7b shows the rate capabilities of the Co/SnO_2 core-shell nanowire arrays at the current densities of 0.1, 0.2, 0.4, 0.8, 1.6, and 3.2 C. The corresponding discharge capacity of was ~ 970, 750, 710, 570, 480, and 350 mAh g^{-1}, respectively. When the current density resets from 6.4 to 0.2 C, the reversible capacity remains 770 mAh g^{-1}. On the other hand, the curves of the electrode "overlapped" well at different current density, exhibiting the charge and discharge process can still be stable at high current density. It is believed that the enhanced performance can be attributed to the core-shell structures, which not only improves the stability of electrode during cycling, but also effectively reduces the volume changes caused by the intercalation and deintercalation of Li^{+}.

As shown in Fig. 8a, the discharge capacity of the planar SnO_2 electrode is only 201.7 mAh g^{-1} with the capacity retention of 22.6% after 100 cycles, while the Co/SnO_2 core-shell nanowire arrays maintain at 667.9 mAh g^{-1} with the capacity retention of 85.7%.

Figure 8b presents the EIS (electrochemical impedance spectroscopy) images of Co/SnO_2 core-shell arrays and planar SnO_2 films, with the amplitude of 1 mV and the frequency range from 600 to 0.01 Hz. Both of the two curves show the similar shape of Nyquist plots, composed of a depressed

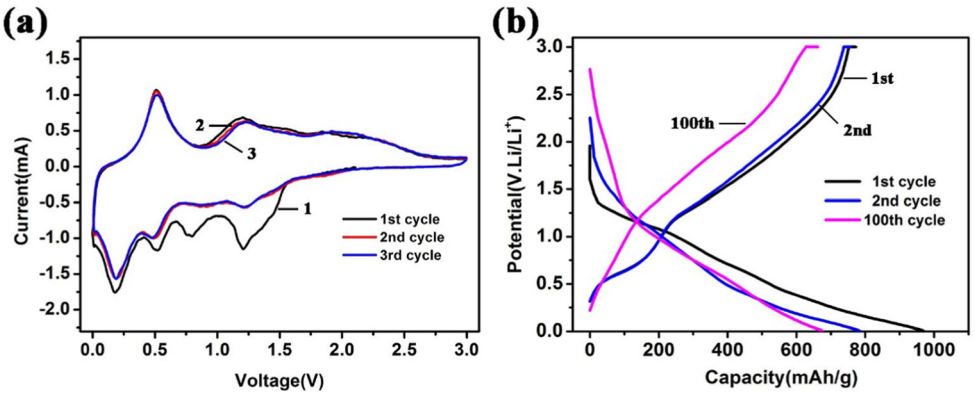

Fig. 6 **a** Cyclic voltammograms of Co/SnO_2 nanowire arrays between 0.01 and 3.0 V at a scan rate of 0.1 mV s^{-1}. **b** Galvanostatic charge/discharge curves for the 1st, 2nd, and 100th cycles

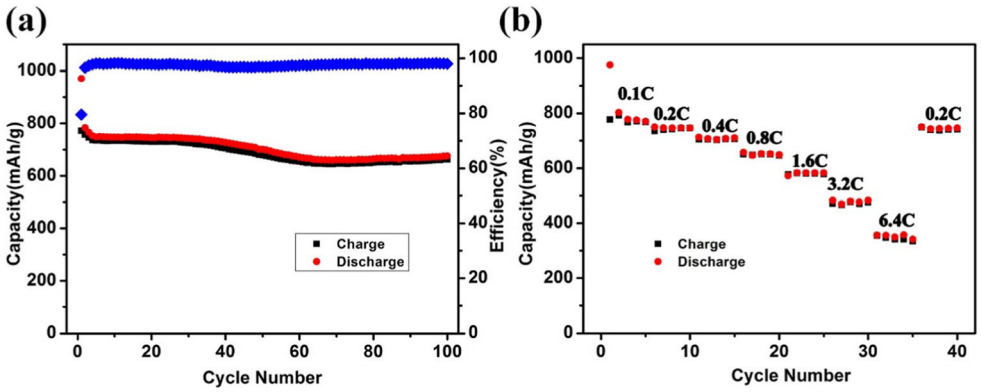

Fig.7 **a** Charge/discharge capacity versus cycle number for the Co/Sno_2 nanowire arrays-based anode materials at a current density of 200 mA g^{-1} at room temperature. **b** Rate capabilities of the Co/SnO_2 nanowire arrays at different current densities

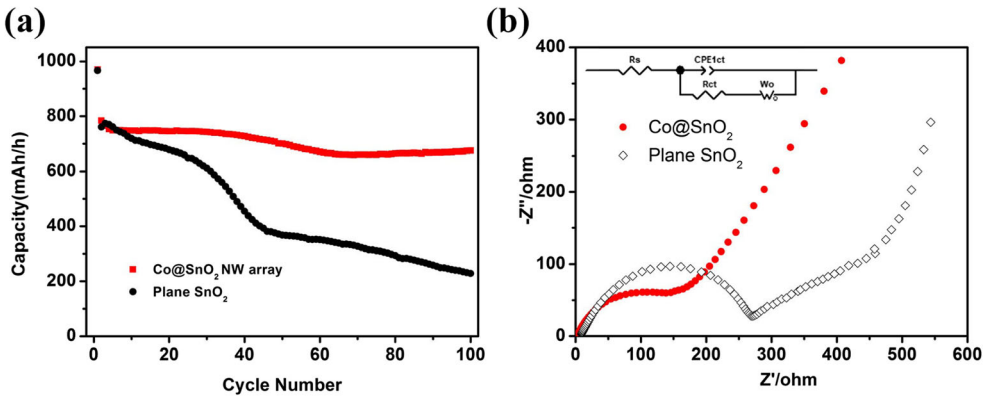

Fig.8 **a** Cycling performance for the Co/SnO_2 nanowire arrays and planar SnO_2 films at a current density of 200 mA g^{-1}. **b** EIS (electrochemical impedance spectroscopy) images of Co/SnO_2 nanowire arrays and planar SnO_2 films

semicircle where a high-frequency semicircle and an inclined line in the low-frequency region [43]. The illustration insertion shows the equivalent circuit of the EIS impedance simulation. Rs represents the internal impedance of the tested LIBs, while Rct and CPE1ct corresponded to charge-transfer resistance and constant phase element of an interface between electrode and electrolyte, respectively. Wo is associated with the Warburg impedance corresponding to the Li-ion diffusion process. As shown in Fig. 8b, the semicircle on the medium-frequency region corresponds the charge-transfer resistance Rct and CPE1ct of the electrode/electrolyte interface, and the inclined line in the low-frequency region corresponds to the lithium-ion diffusion process within the electrode materials. The fitted Rct quantitative values of Co/SnO_2 nanowire arrays and planar SnO_2 films are 270 and 175 Ω, respectively, indicating that the Co nanowire arrays can be acted as current collector network to improve the electrical conductivity and rapid the electron transport during lithiation/delithiation process, resulting in significant improvement in electrochemical performance of Co/SnO_2 nanowire arrays anode. The introduction of metal Co nanowire arrays decreases the distance between electron and collector; thus, the contact impedance and charge transfer impedance are reduced effectively.

Conclusions

Co/SnO_2 nanowire arrays were synthesized via a simple hydrothermal approach, thermal heat treatment, and RF sputtering approaches. When used as anode materials of lithium-ion batteries, the Co/SnO_2 nanowire arrays maintain at 667.9 mAh g^{-1} with the capacity retention of 85.7% after 100 cycles at the current density of 200 mA/g, which was much better than planar SnO_2 film anode. The enhanced electrochemical performance is attributed to the core-shell array nanostructures that can improve the conductivity and buffer the volume changes of tin-based anode. The effect of sputtering time on the morphology and properties of SnO_2 layer was also studied, and the sputtering time of 15 min performed the best cyclic performance.

Acknowledgements The authors would like to thank the financial supports from the Natural Science Foundation of China (Grant Nos. 5 61721005).

References

1. An GM, Na N, Zhang XR, Miao ZJ, Miao SD, Ding KL, Liu ZM (2007) SnO2/carbon nanotube nanocomposites synthesized in supercritical fluids: highly efficient materials for use as a chemical sensor and as the anode of a lithium-ion battery [J]. Nanotechnology 18(43):435707
2. Cao ZZ, Yang HY, Dou P, Wang C, Zheng J, Xu XH (2016) Synthesis of three-dimensional hollow SnO2@PPy nanotube arrays via template-assisted method and chemical vapor-phase polymerization as high performance anodes for lithium-ion batteries [J]. Electrochim Acta 209:700–708
3. Chen LB, Yin XM, Mei L, Li CC, Lei DN, Zhang M, Li QH, Xu Z, Xu CM, and Wang TH (2012) Mesoporous SnO2@carbon core-shell nanostructures with superior electrochemical performance for lithium ion batteries [J]. Nanotechnology 23(3):
4. Chen J, Xia XH, Tu JP, Xiong QQ, Yu YX, Wang XL, Gu CD (2012) Co3O4-C core-shell nanowire array as an advanced anode material for lithium ion batteries [J]. J Mater Chem 22(30):15056–15061
5. Hai W (2014) Novel topotactically transformed carbon-CoO-NiO-NiCo?O? Nanosheet hybrid hetero-structured arrays as ultrahigh performance supercapacitors [J]. Chem Commun (Cambridge, England) 63 50:8697–8700
6. Heo J, Liu Y, Haridas AK, Jeon J, Zhao XH, Cho KK, Ahn HJ, Lee Y, Ahn JH (2018) Carbon-coated ordered mesoporous SnO2 composite based anode material for high performance lithium-ion batteries [J]. J Nanosci Nanotechnol 18(9):6415–6421
7. Idota Y, Kubota T, Matsufuji A, Maekawa Y, Miyasaka T (1997) Tin-based amorphous oxide: a high-capacity lithium-ion-storage material [J]. Science 276(5317):1395–1397
8. Kim C, Jung JW, Yoon KR, Youn DY, Park S, Kim ID (2016) A high-capacity and long-cycle-life lithium ion battery anode architecture: silver nanoparticle-decorated SnO2/NiO nanotubes [J]. ACS Nano 10(12):11317–11326
9. Kong JH, Liu ZL, Yang ZC, Tan HR, Xiong SX, Wong SY, Li X, Lu XH (2012) Carbon/SnO2/carbon core/shell/shell hybrid nanofibers: tailored nanostructure for the anode of lithium ion batteries with high reversibility and rate capacity [J]. Nanoscale 4(2):525–530
10. Lee SH, Noh Y, Kim WB (2017) Convex and concave square arrays of vertical SnO2 nanowire bundles toward lithium-ion storage electrodes [J]. Energy Technol 5(8):1507–1513
11. Leng J, Wang Z, Li X, Guo H, Yan G, Hu Q, Peng W, Wang J (2019) A novel dried plum-like yolk–shell architecture of tin oxide nanodots embedded into a carbon matrix: ultra-fast assembly and superior lithium storage properties [J]. J Mater Chem A 7(10):5803–5810
12. Li T, Li XH, Wang ZX, Guo HJ, Li Y, Wang JX (2017) A new design concept for preparing nickel-foam supported metal oxide microspheres with superior electrochemical properties [J]. J Mater Chem A 5(26):13469–13474
13. Li X, Zhu ZY, Nayaka GP, Duan JG, Wang D, Dong P, Huang L, Zhao JB, Sun SG, Yu XH, Zhang YJ (2018) Self-organized TiO2 network decorated with SnO2 nanoparticles as an anode for lithium-ion batteries [J]. J Alloys Compd 75:268–275
14. Li HJ, Su QM, Kang JW, Huang M, Feng M, Feng HG, Huang P, Du GH (2018) Porous SnO2 hollow microspheres as anodes for high-performance lithium ion battery [J]. Mater Lett 217:276–280
15. Liang SZ, Zhu XF, Lian PC, Yang WS, Wang HH (2011) Superior cycle performance of Sn@C/graphene nanocomposite as an anode material for lithium-ion batteries [J]. J Solid State Chem 184(6):1400–1404
16. Liu JP, Jiang J, Cheng CW, Li HX, Zhang JX, Gong H, Fan HJ (2011) Co3O4 nanowire@MnO2 ultrathin nanosheet core/shell arrays: a new class of high-performance pseudocapacitive materials [J]. Adv Mater 23(18):2076–2081
17. Lou XW, Li CM, Archer LA (2009) Designed synthesis of coaxial SnO2@carbon hollow nanospheres for highly reversible lithium storage [J]. Adv Mater 21(24):2536–2539
18. Madian M, Klose M, Jaumann T, Gebert A, Oswald S, Ismail N, Eychmuller A, Eckert J, Giebeler L (2016) Anodically fabricated TiO2-SnO2 nanotubes and their application in lithium ion batteries [J]. J Mater Chem A 4(15):5542–5552
19. Nishikawa K, Dokko K, Kinoshita K, Woo SW, Kanamura K (2009) Three-dimensionally ordered macroporous Ni-Sn anode for lithium batteries[J]. J Power Sources 189(1):726–729
20. Park MS, Wang GX, Kang YM, Wexler D, Dou SX, Liu HK (2007) Preparation and electrochemical properties of SnO2 nanowires for application in lithium-ion batteries [J]. Angewandte Chemie-International Edition 46(5):750–753
21. Qu J, Li HQ, Henry JJ, Martha SK, Dudney NJ, Xu HB, Chi MF, Lance MJ, Mahurin SM, Besmann TM, Dai S (2012) Self-aligned Cu-Si core-shell nanowire array as a high-performance anode for Li-ion batteries [J]. J Power Sources 198:312–317
22. Shi SL, Liu YG, Zhang JY, Wang TH (2009) Electrochemical properties of SnO2 nanorods as anode materials in lithium-ion battery [J]. Chinese Physics B 18(10):4564–4570
23. Song LX, Yang SJ, Wei W, Qu P, Xu MT, Liu Y (2015) Hierarchical SnO2 nanoflowers assembled by atomic thickness nanosheets as anode material for lithium ion battery [J]. Sci Bull 60(9):892–895
24. Sun X, Huang Y, Zong M, Wu HW, Ding X (2016) Preparation of porous SnO2/ZnO nanotubes via a single spinneret electrospinning technique as anodes for lithium ion batteries [J]. J Mater Sci Mater Electron 27(3):2682–2686
25. Wang JH, Li B, Wu HY, Guo YZ (2008) Synthesis of mesoporous SnO2 and its application in lithium-ion battery [J]. Acta Phys -Chim Sin 24(4):681–685
26. Wang JZ, Du N, Zhang H, Yu JX, Yang DR (2012) Cu-Ge core-shell nanowire arrays as three-dimensional electrodes for high-rate capability lithium-ion batteries [J]. J Mater Chem 22(4):1511–1515
27. Wang C, Zhan Y, Wu L, Li Y, Liu J (2014) High-voltage and high-rate symmetric supercapacitor based on MnO2-polypyrrole hybrid nanofilm [J]. Nanotechnology 25(30):305401
28. Wang H, Wang C, Qing C, Sun D, Wang BX, Qu G, Sun M, Tang YW (2015) Construction of carbon-nickel cobalt sulphide hetero-structured arrays on nickel foam for high performance asymmetric supercapacitors [J]. Electrochim Acta 174:1104–1112
29. Wu L, Zheng J, Wang L, Xiong XH, Shao YY, Wang G, Wang JH, Zhong SK, Wu MH (2019) PPy-encapsulated SnS2 nanosheets stabilized by defects on a TiO2 support as a durable anode material for lithium-ion batteries [J]. Angew Chem Int Ed 58(3):811–815
30. Xie J, Tong L, Su W, Xu Y, Wang LB, Wang YH (2017) Core-shell yolk-shell Si@C@void@C nanohybrids as advanced lithium ion battery anodes with good electronic conductivity and corrosion resistance [J]. J Power Sources 342:529–536
31. Xu YH, Zhu YJ, Liu YH, Wang CS (2013) Electrochemical performance of porous carbon/tin composite anodes for sodium-ion and lithium-ion batteries [J]. Adv Energy Mater 3(1):128–133
32. Xu H, Wang D, Zhang W, Zhu JF, Zhang T, Guo XL, Zhang Y, Sun ZM, Chen J (2018) SnO2 nanorods encapsulated within a 3D interconnected graphene network architecture as high-performance lithium-ion battery anodes [J]. Sustainable Energy & Fuels 2(1):262–270
33. Yan ZL, Hu QY, Yan GC, Li HK, Shih KM, Yang ZW, Li XH, Wang ZX, Wang JX (2017) Co3O4/co nanoparticles enclosed graphitic carbon as anode material for high performance Li-ion batteries [J]. Chem Eng J 321:495–501
34. Yi J, Li XP, Hu SJ, Li WS, Zeng RH, Fu Z, Chen L (2011) TiO2-coated SnO2 hollow spheres as anode materials for lithium ion batteries [J]. Rare Metals 30(6):589–594

35. Zeng H, Zheng M, Skomski R, Sellmyer DJ, Liu Y, Menon L, Bandyopadhyay S (2000) Magnetic properties of self-assembled Co nanowires of varying length and diameter [J]. J Appl Phys 87(9):4718–4720
36. Zhang DA, Wang Q, Wang Q, Sun J, Xing LL, Xue XY (2014) Core-shell SnO2@TiO2-B nanowires as the anode of lithium ion battery with high capacity and rate capability [J]. Mater Lett 128: 295–298
37. Zhang F, Yang CK, Gao X, Chen S, Hu YR, Guan HQ, Ma YR, Zhang J, Zhou HH, Qi LM (2017) SnO2@PANI core-shell nanorod arrays on 3D graphite foam: a high-performance integrated electrode for lithium-ion batteries [J]. ACS Appl Mater Interfaces 9(11): 9620–9629
38. Zhang QB, Chen HX, Luo LL, Zhao BT, Luo H, Han X, Wang JW, Wang CM, Yang Y, Zhu T, Liu ML (2018) Harnessing the concurrent reaction dynamics in active Si and Ge to achieve high performance lithium-ion batteries [J]. Energy Environ Sci 11(3):669–681
39. Zhao B, Huang SY, Wang T, Zhang K, Yuen MMF, Xu JB, Fu XZ, Sun R, Wong CP (2015) Hollow SnO2@Co3O4 core-shell spheres encapsulated in three-dimensional graphene foams for high performance supercapacitors and lithium-ion batteries [J]. J Power Sources 298:83–91
40. Zhao LZ, Wu HH, Yang CH, Zhang QB, Zhong GM, Zheng ZM, Chen HX, Wang JM, He K, Wang BL, Zhu T, Zeng XC, Liu ML, Wang MS (2018) Mechanistic origin of the high performance of yolk@shell Bi2S3@N-doped carbon nanowire electrodes [J]. ACS Nano 12(12):12597–12611
41. Zheng ZM, Wu HH, Chen HX, Cheng Y, Zhang QB, Xie QS, Wang LS, Zhang KL, Wang MS, Peng DL, Zeng XC (2018) Fabrication and understanding of Cu3Si-Si@carbon@graphene nanocomposites as high-performance anodes for lithium-ion batteries [J]. Nanoscale 10(47):22203–22214
42. Zhu CR, Xia XH, Liu JL, Fan ZX, Chao DL, Zhang H, Fan HJ (2014) TiO2 nanotube @ SnO2 nanoflake core-branch arrays for lithium-ion battery anode [J]. Nano Energy 41:05–112
43. Zuo XX, Zhu J, Muller-Buschbaum P, Cheng YJ (2017) Silicon based lithium-ion battery anodes: a chronicle perspective review [J]. Nano Energy 31:113–143